Conodont size in time and space: beyond the temperature-size rule

Catherine Girard, Anne-Lise Charruault, Anne-Béatrice Dufour, Sabrina Renaud

Conodont size in time and space: beyond the temperature-size rule

Catherine GIRARD [a]*, Anne-Lise CHARRUAULT [a], Anne-Béatrice DUFOUR [b], Sabrina RENAUD [b]

a ISEM, Univ Montpellier, CNRS, EPHE, IRD, Montpellier, France (catherine.girard@umontpellier.fr; anne-lise-charruault@umontpellier.fr)

b Laboratoire de Biométrie et Biologie Evolutive (LBBE), UMR 5558 CNRS, Univ Lyon, Université Claude Bernard Lyon 1, Villeurbanne, 69100, France (anne-beatrice.dufour@univ-lyon1.fr ; sabrina.renaud@univ-lyon1.fr)

* Corresponding author:
catherine.girard@umontpellier.fr

ORCID

ABD: 0000-0002-9339-4293

CG: 0000-0003-3123-8276

SR: 0000-0002-8730-3113

Abstract

The Temperature Size Rule (TSR) states that ectoderms display smaller adult body size in warmer conditions. Such a rule may have the potential to explain size response of fossil organisms to past temperature variations, but its validity in deep time has been seldom tested. The generality of this rule was investigated here by compiling data documenting conodont size of three genera (*Palmatolepis, Ancyrodella* and *Polygnathus*) at different spatial and temporal scales during the Late Frasnian and the Famennian, characterized by short- and long-term temperature variations.

The expected TSR was validated in only one out of ten cases. Conodont size was occasionally related to temperature variations, especially during perturbed Late Frasnian time-interval, but the relationship was reverse to the expectations of the TSR. These deviations from the TSR might have several sources. First, size-frequency distributions in the fossil record not only growth patterns but also strategies of reproduction, that may not follow the TSR. Second, limitation in oxygen supply is supposed to be one of the primary drivers of the TSR, but anoxia may interfere with temperature in driving the response to oxygen concentration in the water column. Finally, complex eco-evolutionary dynamics, intermingling threshold response to temperature variation and temperature tolerance of each taxon, may control size evolution. Accordingly, modelling evolutionary modes suggested that size evolution towards new adaptive optima was a predominant pattern of conodont size evolution along the Famennian.

Keywords: Geometric morphometrics, *Palmatolepis*, *Polygnathus*, *Ancyrodella*, Upper Devonian, evolutionary models

Highlights

- Temperature-Size Rule fails to explain most conodont size variations
- A complex interplay of physical and biological factors affected conodont size
- Differential responses of conodont genera could be related to their temperature tolerance

1. Introduction

Body size is a key feature of any organism, reflecting metabolism, physiology, life-history traits and evolutionary history, from unicellular organisms to metazoans (Schmidt et al. 2006). Being easily quantified, its variation in time and space deserved interest since a long time in biology and paleontology. The Bergmann's rule states that populations and species of larger size are found in colder environments (Bergmann 1847). The mechanism beyond being to minimize the surface to volume ratio of an organism in order to limit heat loss, the rule was initially proposed for endotherms (mammals and birds) (Ashton et al. 2000; Rodriguez et al. 2008; Olson et al. 2009; Sun et al. 2017). An extension has been proposed more recently as the "temperature-size rule" (TSR), postulating that ectotherms mature at smaller body sizes when reared in warmer conditions (Atkinson 1994). The response is one of the most taxonomically widespread patterns in biology (Forster et al. 2012), being observed in organisms from bacteria to vertebrates (Atkinson 1994). As a consequence, body-size reduction is considered as a general response to global warming (Sheridan & Bickford 2011).
Oxygen supply has been proposed as a major process beyond the TSR (e.g. Atkinson et al. 2006; Forster et al. 2012; Walczyńska & Sobczyk 2017): cold water can hold more dissolved oxygen than warm water, and as a consequence the dissolved-oxygen concentration is often lower when the water temperature is high. Oxygen supply being more problematic in aquatic than aerial environment, this would explain why the TSR seems particularly well supported in aquatic organisms (Horne et al. 2015, 2017; Rollinson & Rowe 2018).
The TSR acting through very basic metabolic and physiological pathways, it is supposed to be general, and to act across various levels of processes, from specific adaptations to plastic response. It should thus be expressed through space as geographic clines and through time as response to temperature variation (Forster et al. 2012; Salamon et al. 2021). Yet, other processes are susceptible to impact body size, such as food shortage related to primary productivity collapse or interspecific competition (He et al. 2010), possibly leading to deviation from the expected TSR pattern.
Organisms delivering extensive fossil material through sequences documenting temperature changes offer ideal settings to test for the importance of the TSR in deep time (e.g. Schmidt et al. 2006).
The Late Frasnian and the Famennian (Late Devonian, -381 to -360 Ma) are characterized by such changes in sea-water temperatures (Girard et al. 2020; Joachimski et al. 2009; Zhang et al. 2021). The Late Frasnian was characterized by a rapid succession of two anoxic events that were associated with rapid temperature variations (Girard et al. 2007; Joachimski & Buggisch 2002). The Lower Kellwasser event (LKW) was a bio-event of medium importance (Walliser 1996) while the Upper Kellwasser event (UKW), at the Frasnian/Famennian (F/F) boundary, caused a mass extinction among both benthic and pelagic organisms (McGhee 1996). The Famennian, in contrast, was rather characterized

by long term changes in temperature conditions (Joachimski et al. 2009; Zhang et al. 2021). The early Famennian experienced a long-term and stable greenhouse climate, while in the late Famennian, a transition towards an icehouse regime occurred, as premises of the Carboniferous glaciation (Buggisch et al. 2008).

During this period, conodonts delivered an abundant fossil record allowing for quantitative investigation of their size variation. They correspond to an extinct group of marine animals, presumably close to vertebrates (e.g. Aldridge et al. 1993; Janvier 1995). Because of the presence of developed eyes and fins, they have been interpreted as nektonic organisms with active swimming (Briggs et al. 1983; Purnell 1994). The most commonly preserved parts of these organisms are microscopic elements which composed a complex feeding apparatus (Purnell 1994; Donoghue & Purnell 1999) allowing them to exploit a trophic niche of first level consumers (Shirley et al. 2018; Balter et al. 2019).

Among the different types of elements composing the apparatus, the platform element (P1) displayed a rapid morphological evolution making it widely studied for biostratigraphic purposes (e.g. Spalletta et al. 2017; Ziegler & Sandberg 1990). These elements grew by addition of thin lamellae throughout the animal's life, and thus presumably constitute a proxy of body size (Purnell 1994). While the species concept remains debated in this group of extinct organisms with extensive morphological variation (Scott & Collinson 1959; Koike 1988; Girard et al. 2004), genera can be easily recognized and may constitute a robust unit to assess size changes, including plastic response, evolution, and possibly cryptic species composition (Girard et al. 2004). Using such an approach at the generic level, it has been suggested that conodont size tracked temperature changes during the Frasnian, in areas corresponding nowadays to China (Zhang et al. 2020). The question rises whether this observation, congruent with the TSR, can be generalized to size variations in conodonts in other time intervals and in other areas.

The size-frequency distribution of the P1 elements of three genera was therefore quantified using geometric morphometrics methods (Renaud et al. 1999; Renaud et al. 2021). By comparing size values across time (along sections) and space (by comparing sections), the following hypotheses where investigated.

(1) TSR as general driver of conodont size variation should lead to congruent signatures among different genera, across time and space, and at various time scales.
(2) Alternatively, crises as cause of size reduction (Twitchett 2006) should lead to deviation from the TSR. The response to the UKW event during the Late Frasnian might correspond to such a situation of interfering factors blurring the TSR response.

2. Material

The conodont elements considered in this study come from sections located in different parts of the world. Most of the sampling was located in Montagne Noire (France): Coumiac Upper Quarry (CUQ), La Serre trench C (LSC) and Col des Tribes (CT). Samples from Buschteich (BU, Thuringia, Germany), Mrirt (Moroccan Meseta, Morocco) and Xom Nha (XN, Central Vietnam) complemented this sampling (Fig. 1).

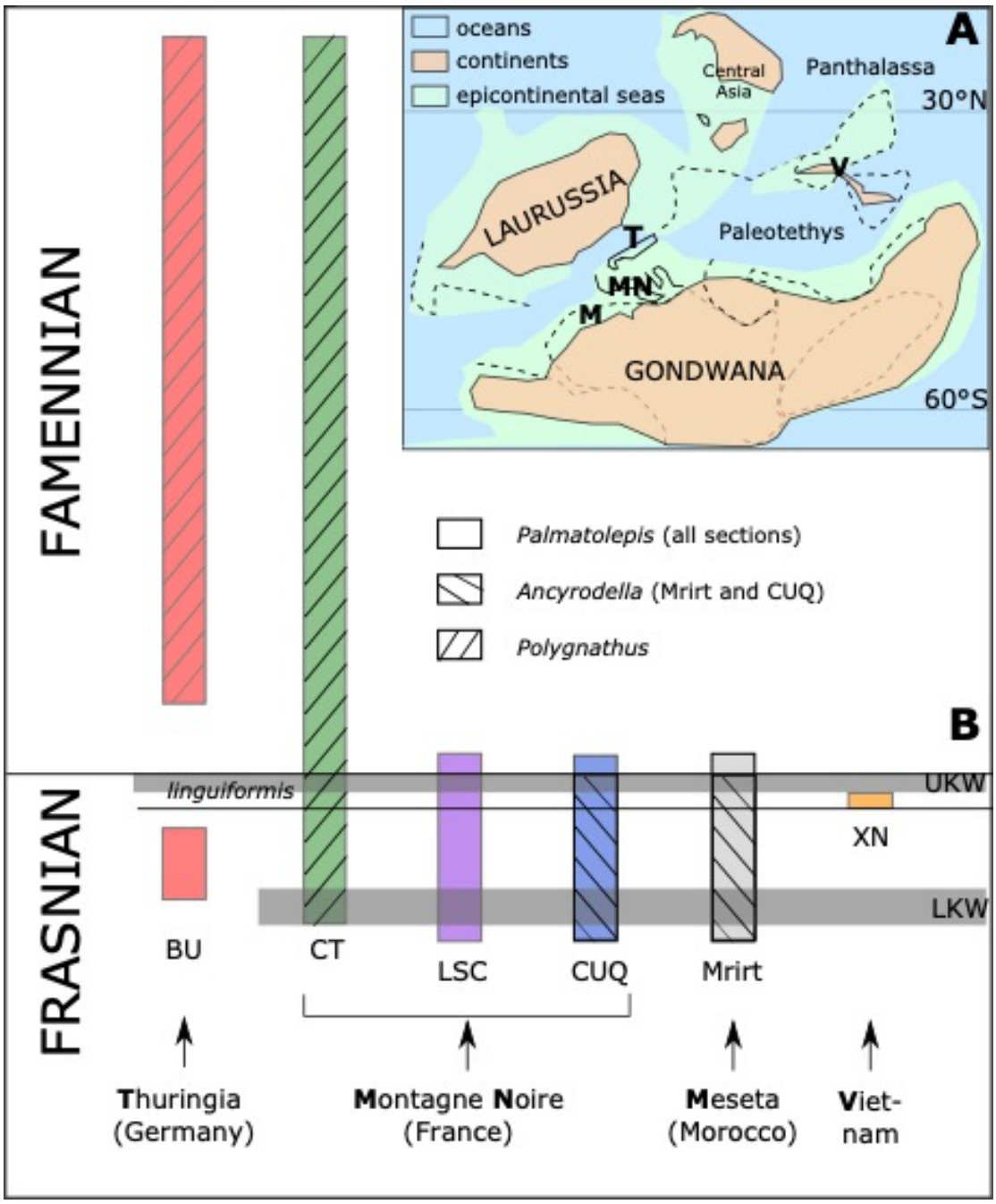

Figure 1. A. Schematic paleogeographic map of the Late Devonian. T: Thuringia (Germany); MN: Montagne Noire (France); M: Meseta (Morocco); V: Central Vietnam. B. Stratigraphic extension of the studied sections (BU: Buschteich, CT: Col des Tribes, CUQ: Coumiac Upper Quarry, LSC: La Serre Trench C, XN: Xom Nha). In dark grey, the Lower (LKW) and Upper (UKW) Kellwasser events.

Three conodont genera occurring through all or part of the Upper Devonian were considered in the present study: *Ancyrodella*, *Palmatolepis*, and *Polygnathus* (Fig. 2). The stratigraphic extension of *Ancyrodella* was limited to the Frasnian, with its extinction coinciding with the F/F boundary. *Palmatolepis* stratigraphic extension covered the whole Upper Devonian, its extinction occurring at the end of the Famennian. *Polygnathus* was known during all the Devonian.

In order to study morphological variations on a broad geographical scale, the time-slice corresponding to the *linguiformis* Zone (last Zone of the Frasnian, Ziegler & Sandberg 1990) was selected. *Palmatolepis* size data were available from the literature (Girard et al. 2010), allowing for a comparison including samples located in the West (sections from Mrirt and from the Montagne Noire) and in the East (Vietnam) of the Paleotethys (Fig. 1). Three levels were included for Mrirt, two levels for CUQ, two levels for CT, and two levels for Xom Nha.

Short-term size variations of conodonts were documented in the period of the Late Frasnian and early Famennian, encompassing environmental perturbations around the Lower and Upper Kellwasser events. This period was thereafter designed as the “whole Kellwasser period”. *Palmatolepis* size variations were considered in CUQ, LSC and Mrirt (Girard et al. 2007). *Ancyrodella* was further considered during the same period, with the difference that its extinction at the F/F boundary limited its sampling to the Late Frasnian. Size variations were documented in CUQ and Mrirt (Girard et al. 2008).

Long-term temporal variations were assessed along two Famennian sequences at the Col des Tribes (CT) and the Buschteich sections (BU) for *Palmatolepis* and *Polygnathus*. Few Frasnian levels were included in CT. Samples correspond to those considered in stratigraphic analyses (Girard et al. 2014, 2017), in a study comparing temperature and water-depth variations in both sections (Girard et al. 2020), and in a study devoted to *Polygnathus* morphological evolution over this time period (Renaud et al. 2021).

Oxygen isotope data, used as paleotemperature proxies, were available from previously published data (Balter et al. 2008; Le Houedec et al. 2013; Girard et al. 2020). Furthermore, ecological preferences of conodont genera are supposed to be dependent on water depth (Seddon & Sweet 1971; Klapper & Barrick 1975) rather than on temperature. *Palmatolepis* being considered as off-shore dweller and then associated with deep waters, its percentage in the conodont assemblages was considered as a proxy of water-depth variations through the Famennian (Girard et al. 2020), in order to test an alternate candidate for external forcing on conodont size variation.

3. Methods

3.1. Size estimates

3.1.1. Outline analysis: Palmatolepis *and* Ancyrodella. – A method based on Fourier outline analysis was applied to quantify the form (size + shape) of the element platform (P1) for *Palmatolepis* (Renaud & Girard 1999; Girard et al. 2010; Girard & Renaud 2012) and *Ancyrodella* (Girard & Renaud 2008) (Fig. 2). According to this method, the 2D platform outline was automatically digitized using an image analyzer (Optimas v. 6.0) and 64 points were sampled at equally-spaced intervals along the outline, the starting point being defined at the termination of the blade. From these coordinates, 64 radii were calculated, corresponding to the distance of each point to the center of gravity (centroid) of the outline. A Fourier transform was then applied to this set of 64 radii expressed as a function of the cumulated curvilinear abscissa along the outline, decomposing the empirical outline as a sum of trigonometric functions of decreasing wavelength. Size was calculated as the zero harmonic (A0), corresponding to the size of the best-fitting circle to the original outline. This procedure is implemented as "sfourier" in Momocs (Bonhomme et al. 2014).

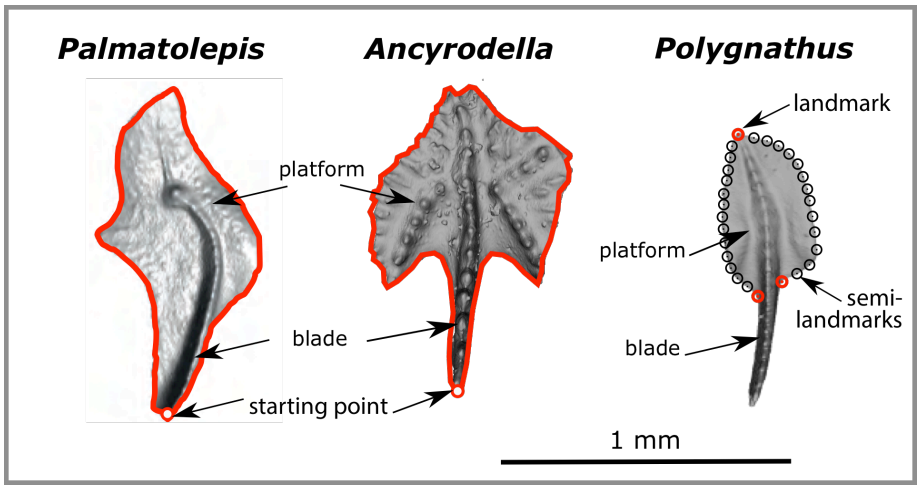

Figure 2. The P1 elements of the three genera considered in this study, with a schematic representation of the method used for size quantification. *Palmatolepis, Ancyrodella*: in red, the outline sampled by 64 points. *Polygnathus*: red dots: landmarks, open dots: sliding semi-landmarks.

3.1.2. Landmark-based estimate of Polygnathus *size*. – The description of *Polygnathus* 2D shape did not include the blade, too frequently damaged on the collected specimens. Hence, the outline of the (P1) platform was not closed, precluding the use of Fourier methods; landmark-based descriptors were used instead (Fig. 2). Three landmarks and two series of 13 semi-landmarks were manually digitized on the edges of the platform (Renaud et al. 2021). The size of the platform was estimated as the centroid size (CS) of the configuration, defined as the square root of the sum of squared distances of all landmarks to their centroid (Slice et al. 1996).

Since size distributions were skewed towards large size (Girard et al. 2004; Girard et al. 2010), size estimates were log-transformed for all analyses. Sample size and summary statistics are provided as Supplementary Tables 1 to 10.

3.1.3. Statistical analyses

Within each section, or within the *linguiformis* time-slice, size difference between levels were tested using Kruskall-Wallis tests, completed by pairwise Wilcoxon tests between applied to successive levels.

Mean size were calculated for each level. Within each section, or within the *linguiformis* time-slice, Pearson correlations were performed between these group means and the corresponding isotopic value ($\delta^{18}O$).

Correlations between variables can however arise due to temporal autocorrelation. This possible effect was assessed using a first-order autoregressive (AR1) model using generalized least squares (gls) (Rita et al. 2019). This corresponds to using the order of the observations in the data as a covariate.

Such correlations on means per level however neglect the fact that sample size and variance are heterogeneous among levels. One way to circumvent this issue is to consider that all conodonts from a given level represent a random sample from the original population. They experienced similar growing conditions, that may have led to a pseudo-correlation between them, possibly blurring the correlation of interest with paleotemperature. Models with linear mixed effects (lme) were therefore constructed, considering size as a function of temperature, with levels as random effect. A last series of models further included first-order autocorrelation. These models were fitted using the package nlme (Pinheiro et al. 2018).

3.1.4. Evolutionary models

Using as entry data the size mean and variance per level as well as the estimated age, evolutionary models were fitted to the data using the paleoTS package (Hunt 2014). The models considered were the following.

- Stasis, with a constant mean and variance (Sheets & Mitchell 2001);
- General random walk (GRW), where each “step" is drawn from a distribution with a non-zero mean, corresponding to the directionality of the trend (Hunt 2006; Hunt & Carrano 2010);
- Unbiased random walk (URW), corresponding to non-directional random walk (steps drawn from a distribution with a zero mean) (Hunt 2006);
- Ornstein-Uhlenbeck (OU), corresponding to the evolution towards an adaptive peak (Hansen 1997; Butler & King 2004; Beaulieu et al. 2012, Hunt et al. 2008);

- One punctuation along the sequence: all shift points are tested, with the constraint that the number of steps in each segment is larger than a given threshold n (here, the value by default n=7 was retained) (Hunt 2016).
- Several models considered that the mode of trait evolution shifted once along the sequence. The minimum number of steps in a segment was retained as n=7.
    - URW-Stasis and Stasis-URW: first evolution according to an unbiased random walk and then stasis (or the reverse);
    - GRW-Stasis and Stasis-GRW: first evolution according to an unbiased random walk and then stasis (or the reverse).

Finally, a model where evolution tracks a covariate was considered (Hunt et al. 2010). This allowed to test for size covarying with the paleotemperature proxy $\delta^{18}O$. To test an alternate model of environmental forcing, the percentage of *Palmatolepis* in the assemblage was considered (Girard et al. 2020), supposedly tracing water depth variations. These models were only considered for the evolution along the Famennian.

The constraint on the minimum number of steps in a segment precluded to estimate two-segments models for several sequences that were documented by too few levels.

All models were estimated using a full likelihood approach ("Joint"). The Akaike information criterion (AIC) estimated the quality of each model; based on the number of parameters and the Log-likelihood of the model. The corrected criterion (AICc) was calculated from the AIC test by correcting for small sample sizes. The preferred model is the one with the minimum AICc value. While comparing several models, two other parameters were provided to help identifying the preferred one: dAICc, corresponding to the difference in AICc score between the best model and the model being compared, and Akaike weight (Akaike.wt), corresponding to the proportion of the total amount of predictive power provided by the full set of models, contained in the model being assessed.

All analyses were performed under R (R-Core-Team 2018).

4. Results

4.1. Size distribution in the different genera and sections

Conodont size distributions differed in the four sections considered for the *linguiformis* zone ($P < 0.0001$). Mrirt displayed more abundant small-sized *Palmatolepis* specimens than the other outcrops (Fig. 3A). When considering the "whole Kellwasser period", size differed as well between the three outcrops considered ($P < 0.0001$) but the most abundant small sized *Palmatolepis* elements were found in LSC. Regarding *Ancyrodella*, no size difference was observed between the two sections involved ($P = 0.8055$) (Fig. 3B).

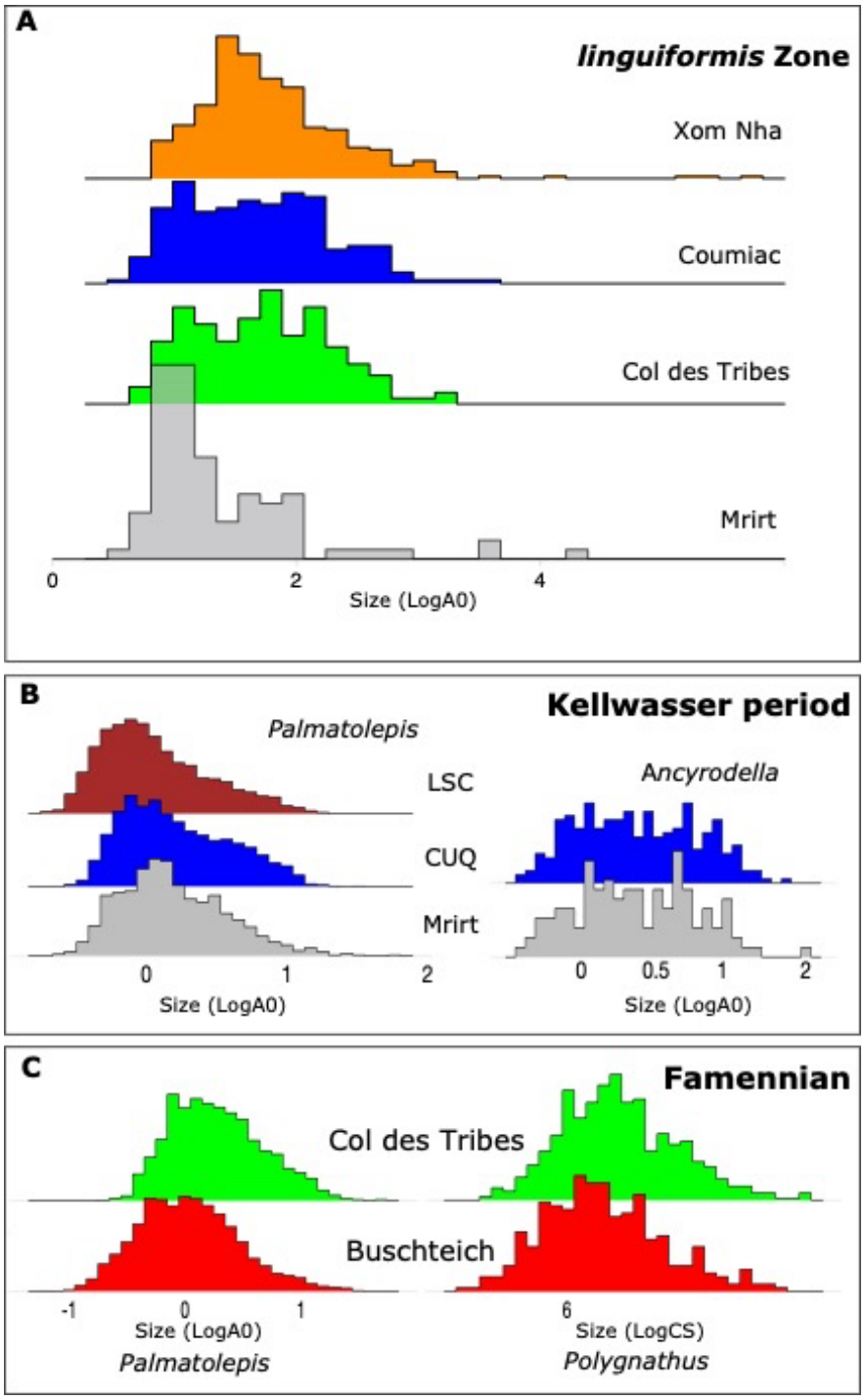

Figure 3. Size frequency-distribution of the conodont P1 elements for the three periods considered. (**A**) Distribution of *Palmatolepis* size per section in the « *linguiformis* » time-slice. (**B**) Distribution per section for *Palmatolepis* and *Ancyrodella* over the « whole Kellwasser period ». (**C**) Distribution per section over the Famennian for *Palmatolepis* and *Polygnathus*. *Palmatolepis* and *Ancyrodella* size is estimated as the zero harmonic (A0) of a Fourier analysis of the platform outline. *Polygnathus* size is estimated as the Centroid Size (CS) of landmark configurations. All data were log-transformed. CUQ: Coumiac Quarry, LSC: La Serre Trench C.

Considering the Famennian record, *Palmatolepis* elements were smaller in BU than in CT (P < 0.0001). The difference was also significant when considering *Polygnathus* (P = 0.0002) and the pattern was similar, with elements tending to be smaller in BU than in CT (Fig.3C).

4.2. Differences between levels along sections

Significant size differences among levels were found in the *linguiformis* data set (Table 1) and along all sections and genera, except for *Ancyrodella* at Mrirt (Table 2, Supplementary Tables).

In the *linguiformis* time slice, the difference was mostly driven by Mrirt levels being different from most other samples. Pairwise Wilcoxon tests among successive levels along sections showed that significant differences were scattered all over the record for *Palmatolepis* in CUQ, Mrirt and LSC during the Kellwasser period, and all along the Famennian in CT and BU. Only few differences were significant between the two Kellwasser events for *Ancyrodella* in CUQ, and few differences towards the end of the Famennian were significant for *Polygnathus* in CT (Supp. Tables 1 to 10).

Table 1. Differences between levels in the *linguiformis* time-slice. Non-adjusted probabilities of pairwise Wilcoxon tests are provided. In bold, P < 0.01, in italics P < 0.05. CT: Col des Tribes; CUQ: Coumiac Upper Quarry; M: Mrirt; XN: Xom Nha.

	CT22	CT23	CUQ31f	CUQ31g1	CUQ31g2	M09	M11a	M11b	XN52-1
CT23	0.3493								
CUQ31f	0.1220	0.9620							
CUQ31g1	0.5458	0.7090	0.5180						
CUQ31g2	0.7678	0.4717	0.1939	0.5423					
M09	**0.0000**	**0.0009**	**0.0000**	**0.0000**	**0.0001**				
M11a	*0.0173*	0.1020	0.0664	*0.0497*	0.0580	0.9673			
M11b	**0.0058**	0.0950	0.0523	*0.0306*	*0.0358*	0.2466	0.4653		
XN52-1	0.3395	0.6519	0.2978	0.9071	0.3192	**0.0000**	*0.0204*	**0.0098**	
XN53-1	0.3649	0.0688	**0.0033**	0.1317	0.7107	**0.0000**	**0.0042**	**0.0004**	*0.0198*

Table 2. Differences in size between levels, and summary of Pearson correlations between mean size and $\delta^{18}O$ in the different cases considered. N tot: total number of specimens; P KW: probabilities of size differences between levels, based on Kruskal Wallis tests; N mean: number of levels; P: probabilities of correlation between mean size and $\delta^{18}O$ per level; R: Pearson coefficient of correlation; range Size: range between minimum and maximum mean size values; range $\delta^{18}O$: range between minimum and maximum $\delta^{18}O$ values. Kellwasser: “whole Kellwasser period”. In bold, P < 0.01, in italics P < 0.05.

Period	Genus	Section	N tot	P KW	N mean	Pcor.test	R	Range Size	Range $\delta^{18}O$
linguiformis	*Palmatolepis*		830	**<0.00001**	10	**0.0031**	0.8277	0.3816	4
Kellwasser	*Palmatolepis*	CUQ	2625	**<0.00001**	19	*0.0109*	-0.5696	0.4557	1.66
		M	1295	**0.00005**	13	0.2069	0.3749	0.3220	1.3
		LSC	3178	**<0.00001**	21	0.8040	0.0576	0.5836	1.78

	Ancyrodella	CUQ	283	**0.00493**	17	0.1797	-0.3415	0.8667	1.66
		M	124	0.15770	8	0.3452	-0.3858	0.3985	1.3
Famennian	*Palmatolepis*	CT	2229	**<0.00001**	26	*0.0374*	-0.4102	0.5812	2.1
		BU	4370	**<0.00001**	26	0.1628	-0.2820	0.5823	1.5
	Polygnathus	CT	745	**<0.00001**	21	0.9858	0.0041	0.7155	2.1
		BU	347	**0.00001**	17	0.7692	0.0726	1.0850	1.2

4.3. Correlations between mean size and $\delta^{18}O$

Among the ten datasets considered, the expected relationship according to the TSR (positive correlation between size and $\delta^{18}O$) was only supported in the case of the geographic variation in the *linguiformis* time slice (Fig. 4; Table 2).

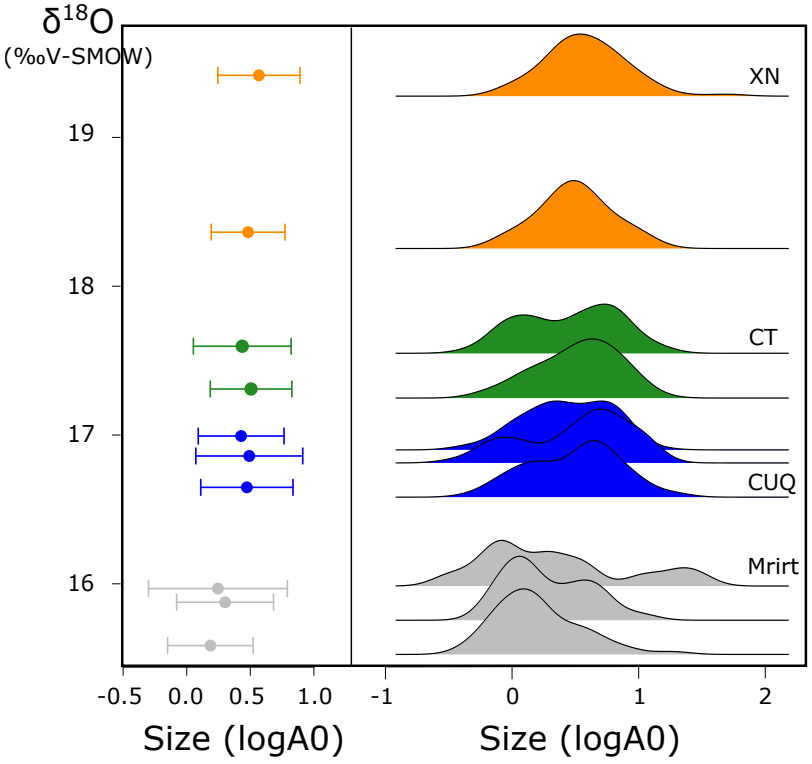

Figure 4. *Palmatolepis* size as a function of $\delta^{18}O$ in the "*linguiformis*" time-slice. A. Mean size per level ± standard deviation (SD). B. Size frequency distribution of *Palmatolepis* size (LogA0) as a function of $\delta^{18}O$. CUQ: Coumiac Upper Quarry, CT: Col des Tribes, XN: Xom Nha.

Only two other correlations were significant, but with a negative relationship between mean size and $\delta^{18}O$. They involved *Palmatolepis* during the Kellwasser period at CUQ (Fig. 5C), and along the Famennian at CT (Fig. 6B).

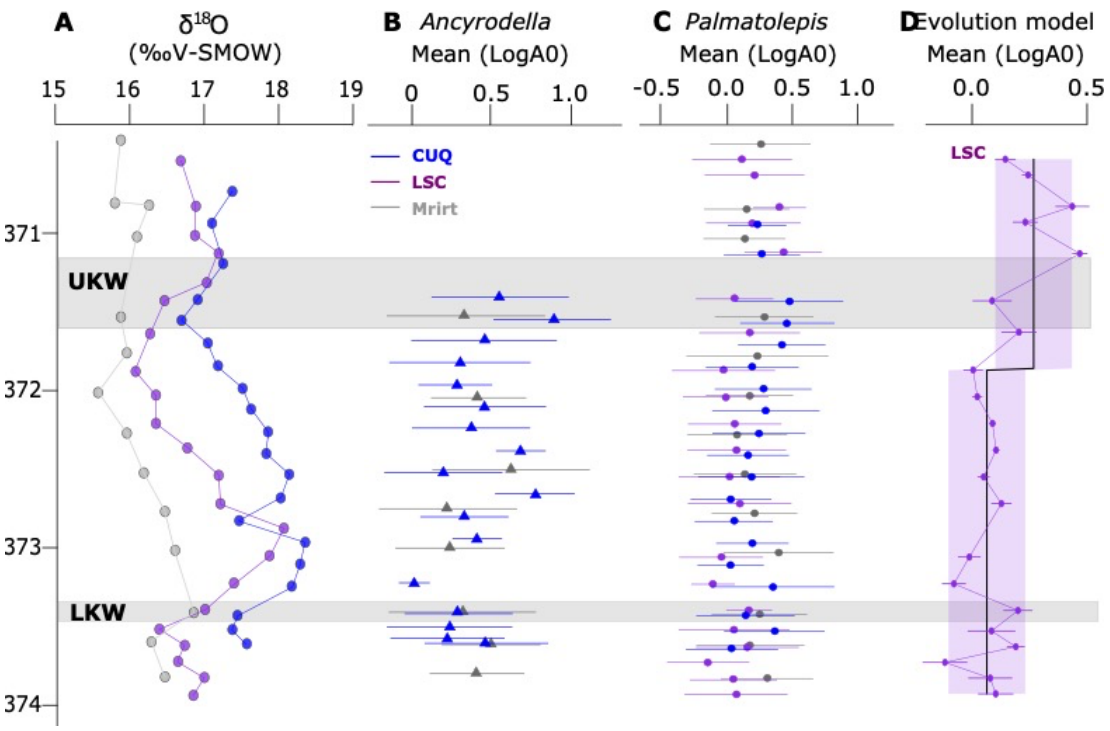

Figure 5. Paleotemperature proxy and conodont size variation during the "whole Kellwasser period". A. $\delta^{18}O$ variations. B. *Ancyrodella* mean size ± SD. C. *Palmatolepis* mean size ± SD. D. One punctuation as best-fitting model for size evolution of *Palmatolepis* at LSC. Mrirt in grey, LSC in violet, CUQ in blue. Dots: circles, *Palmatolepis*; triangles, *Ancyrodella*. Grey boxes: Lower and Upper Kellwasser events.

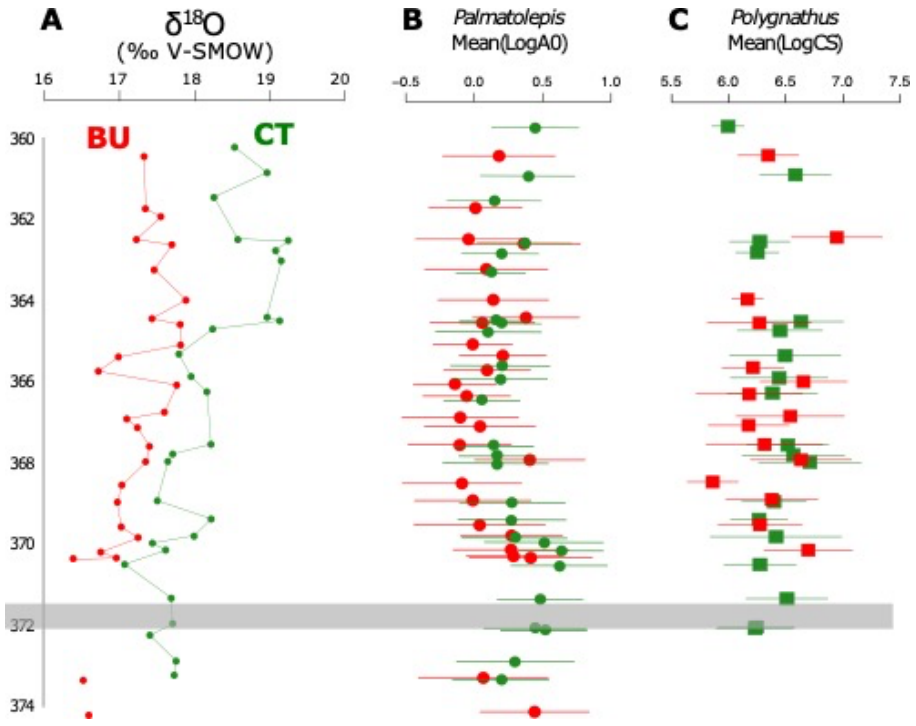

Figure 6. Paleotemperature proxy and conodont size variation during the "Famennian period". A. $\delta^{18}O$ variations. B. *Palmatolepis* mean size (logA0) per level ± SD. C. *Polygnathus* mean centroid size (logCS) per level

± SD. Circles: *Palmatolepis*, squares: *Polygnathus*. CT in green, BU in red. The grey box represents the Upper Kellwasser event.

4.4. Investigating temporal autocorrelation and levels as random effects

The different models considered as alternate to the basic Pearson correlation (Table 2) provided overall congruent results (Table 3). Variation between size and temperature was supported during the "*linguiformis"* time-slice, and in most of the case for *Palmatolepis* during the Kellwasser period at CUQ. This correlation was only marginally significant, however, when considering the linear mixed effects model with temporal auto-correlation. The same was true for *Palmatolepis* in the CT Famennian record, where the size – $\delta^{18}O$ relationship was consistently significant except when considering the gls model on mean values corrected for auto-correlation. The size-$\delta^{18}O$ relationship emerged as significant for *Ancyrodella* at CUQ only when considering the lme model.

Table 3. Summary of the models exploring the correlation between Log size and $\delta^{18}O$ in the different cases considered. First line indicates if models were performed on the means or on all specimens. Probabilities are provided for the following models: Pearson correlation on the means per level; gls on the means per level, including first-order autocorrelation; lme on all specimens including levels as a random effect; the same models including first-order autocorrelation. Models including first-order autocorrelation are not provided for the *linguiformis* time-slice, since time is not involved. Palm: *Palmatolepis*; Ancyro: *Ancyrodella*, Poly: *Polygnathus*; KW: whole Kellwasser period; CUQ: Coumiac; M: Mrirt; LSC: La Serre, CT: Col des Tribes; BU: Buschteich. In bold, P < 0.01, in italics P < 0.05.

	means		all specimens	
	cor.test	gls - corAR1	lme | Level	lme | Level - corAR1
linguiformis	**0.0031**		**0.0001**	
Palm_KW_CUQ	*0.0109*	**0.0004**	**0.0074**	0.0967
Palm_KW_M	0.2069	0.2935	0.2070	0.5872
Palm_KW_LSC	0.8040	0.4887	0.6584	0.1699
Ancyro_CUQ	0.1797	0.1822	*0.0319*	0.1745
Ancyro_M	0.3452	0.3680	0.3693	0.8439
Palm_Fam_CT	*0.0374*	0.8715	*0.0252*	*0.0357*
Palm_Fam_BU	0.1628	0.1938	0.1663	0.2406
Poly_Fam_CT	0.9858	0.9339	0.9562	0.9441
Poly_Fam_BU	0.7626	0.7421	0.9404	0.9495

4.5. Testing evolutionary modes

Given the constraints of minimum seven steps per segment, two-segments models were only tested when 19 or more levels were available along a section (*Palmatolepis* CUQ and LSC during the Kellwasser, CT and BU along the Famennian; *Polygnathus* at CT).

342 *4.5.1. Whole Kellwasser period,* Palmatolepis. – In CUQ, the best model by far pointed to size
343 evolution tracking $\delta^{18}O$ variations along the section (Table 4). In Mrirt, the best model among the few
344 tested emerged as the stasis (Table 5). In LSC (Table 6), the best model involved one punctuation
345 located at step 14 (LSC14b). Accordingly, *Palmatolepis* elements tended to reach larger size towards
346 the end of the record (Fig. 5D).
347
348 Table 4. Comparison of support for each model of *Palmatolepis* evolution in CUQ (comparing 10 models [n =
349 19, method = joint]. LogL = model log likelihood, K = number of model parameters, AICc = Akaike's Information
350 Criterion corrected for small sample size, dAICc = difference in AICc score between the best model and the
351 model being compared, Akaike.wt: Akaike weights (proportion of the total amount of predictive power).

	LogL	K	AICc	dAICc	Akaike.wt
GRW	12.65087	3	-17.701743	5.0689095	0.032
URW	12.56427	2	-20.378539	2.3921128	0.122
Punc-1	16.35977	4	-21.862401	0.9082516	0.257
OU	15.03664	4	-19.216147	3.5545050	0.068
Stasis	10.75232	2	-16.754644	6.0160081	0.020
URW-Stasis	13.66500	5	-12.714623	10.0560287	0.003
Stasis-URW	15.19252	4	-19.527894	3.2427580	0.080
GRW-Stasis	13.79502	6	-8.590034	14.1806180	0.000
Stasis-GRW	13.79502	5	-15.882376	6.8882759	0.013
$\delta^{18}O$	**15.18533**	3	**-22.770652**	**0.0000000**	**0.405**

352
353 Table 5. Comparison of support for each model of *Palmatolepis* evolution in Mrirt (comparing 5 models [n = 13,
354 method = joint]. LogL = model log likelihood, K = number of model parameters, AICc = Akaike's Information
355 Criterion corrected for small sample size, dAICc = difference in AICc score between the best model and the
356 model being compared, Akaike.wt: Akaike weights (proportion of the total amount of predictive power).

	logL	K	AICc	dAICc	Akaike.wt
GRW	11.67972	3	-14.69278	6.818228	0.018
URW	11.67321	2	-18.14642	3.364583	0.103
OU	14.78178	4	-16.56356	4.947449	0.047
Stasis	**13.3555**	**2**	**-21.511**	**0.000000**	**0.556**
$\delta^{18}O$	14.38439	3	-20.10211	1.408892	0.275

357
358
359 Table 6. Comparison of support for each model of *Palmatolepis* evolution in LSC (comparing 10 models [n = 21,
360 method = joint]. LogL = model log likelihood, K = number of model parameters, AICc = Akaike's Information
361 Criterion corrected for small sample size, dAICc = difference in AICc score between the best model and the
362 model being compared and Akaike.wt: Akaike weights (proportion of the total amount of predictive power).

	logL	K	AICc	dAICc	Akaike.wt

GRW	11.56475	3	-15.71773	10.020576	0.005
URW	11.55291	2	-18.43916	7.299153	0.020
Punc-1	**18.11915**	**4**	**-25.73831**	**0.000000**	**0.757**
OU	13.82143	4	-17.14286	8.595449	0.010
Stasis	11.52432	2	-18.38198	7.356329	0.019
URW-Stasis	16.07685	5	-18.1537	7.584605	0.017
Stasis-URW	16.43132	4	-22.36264	3.375668	0.140
GRW-Stasis	16.17297	6	-14.34594	11.392364	0.003
Stasis-GRW	16.40713	5	-18.81425	6.924054	0.024
$\delta^{18}O$	11.56613	3	-15.7205	10.017807	0.005

4.5.2. Whole Kellwasser period, Ancyrodella. – Two models were almost equally performant for this record, suggesting either a stasis, or an evolution of size coupled to the paleotemperature proxy (Table 7).

Table 7. Comparison of support for each model of *Ancyrodella* evolution in CUQ (comparing 5 models [n = 17, method = joint]. LogL = model log likelihood, K = number of model parameters, AICc = Akaike's Information Criterion corrected for small sample size, dAICc = difference in AICc score between the best model and the model being compared and Akaike.wt: Akaike weights (proportion of the total amount of predictive power).

	logL	K	AICc	dAICc	Akaike.wt
GRW	-0.4723795	3	8.7909128	7.875884	0.010
URW	-0.5474194	2	5.9519817	5.036953	0.040
OU	2.7027708	4	5.9277918	5.012763	0.041
Stasis	**1.9710571**	**2**	**0.9150286**	**0.000000**	**0.499**
$\delta^{18}O$	**3.2678661**	**3**	**1.3104216**	**0.395393**	**0.410**

4.5.3. Famennian record, Palmatolepis. – Along the Famennian record in CT, the best model fitting *Palmatolepis* evolution corresponded to a shift from an unbiased random walk to stasis (Table 8), occurring at step 8 (CT34, 369.7 Ma). In BU, one model also emerged clearly, corresponding to one punctuation (Table 9) occurring at step 7 (BU21, 369.3 Ma). Both shifts appear thus to be almost perfectly congruent, despite being estimated independently in the two sections. In both cases, the shift corresponded to smaller *Palmatolepis* size in the second part of the record (Figure 7A).

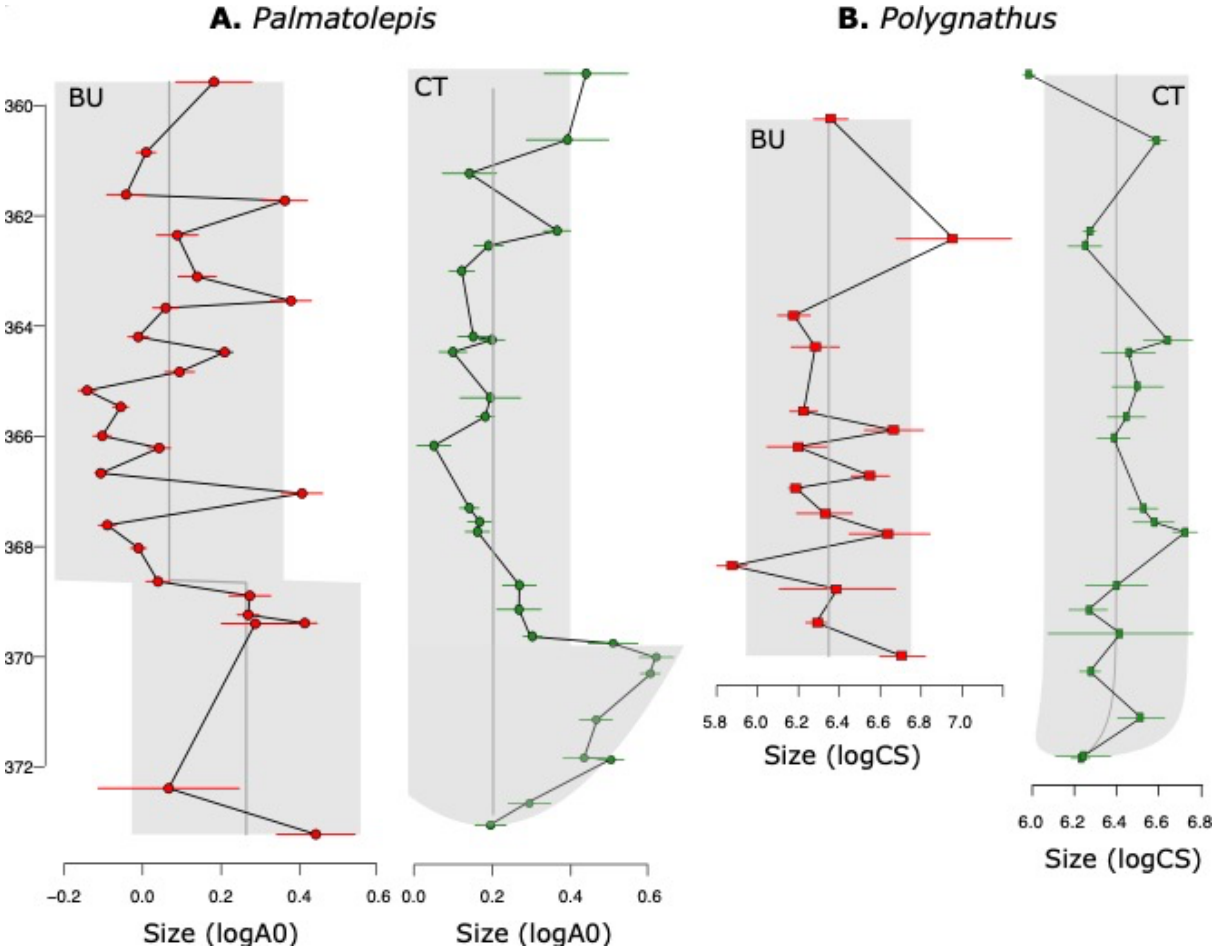

Figure 7. A. Models of evolution for *Palmatolepis* size along the Famennian. BU: the best-fitting model corresponded to one punctuation. CT: the best-fitting model corresponded to a shift from URW to stasis; the one-punctuation model provides a visualization of the shift in evolutionary mode. B. Models of evolution for *Polygnathus* size along the Famennian. BU: The best-fitting model corresponded to a stasis. CT: The best-fitting model corresponded to a Ohrstein-Uhlenbeck model, corresponding to an initial evolution towards an adaptive peak, followed by stability around this peak.

Table 8. Comparison of support for each model of *Palmatolepis* evolution in CT (comparing 11 models [n = 26, method = joint]. LogL= model log likelihood, K = number of model parameters, AICc = Akaike's Information Criterion corrected for small sample size, dAICc = difference in AICc score between the best model and the model being compared and Akaike.wt: Akaike weights (proportion of the total amount of predictive power).

	logL	K	AICc	dAICc	Akaike.wt
GRW	18.10755	3	-29.1242	7.9418906	0.010
URW	18.0473	2	-31.57285	5.4932343	0.034
Punc-1	19.88463	4	-29.86451	7.20158	0.015
OU	20.05839	4	-30.21203	6.8540608	0.017
Stasis	10.21039	2	-15.89905	21.1670384	0.000
URW-Stasis	**25.03304**	**5**	**-37.06609**	**0.000000**	**0.533**

Stasis-URW	18.83415	4	-27.76354	9.3025436	0.005
GRW-Stasis	*26.41616*	*6*	*-36.41127*	*0.6548168*	*0.384*
Stasis-GRW	18.84199	5	-24.68398	12.3821035	0.001
$\delta^{18}O$	12.93283	3	-18.77475	18.2913371	0.000
p□□□	10.22268	3	-13.35444	23.7116426	0.000

Table 9. Comparison of support for each model of *Palmatolepis* evolution in BU (comparing 11 models [n = 26, method = joint]. LogL= model log likelihood, K = number of model parameters, AICc = Akaike's Information Criterion corrected for small sample size, dAICc = difference in AICc score between the best model and the model being compared, Akaike.wt: Akaike weights (proportion of the total amount of predictive power).

	logL	K	AICc	dAICc	Akaike.wt
GRW	-1.258698	3	9.608306	21.960669	0.000
URW	-1.273532	2	7.068803	19.421166	0.000
Punc-1	**11.128563**	**4**	**-12.352363**	**0.000000**	**0.295**
OU	10.68761	4	-11.470458	0.881905	0.190
Stasis	7.894902	2	-11.268065	1.084298	0.171
URW-Stasis	10.366653	5	-7.733307	4.619056	0.029
Stasis-URW	2.279478	4	5.345807	17.69817	0.000
GRW-Stasis	10.884588	6	-5.348124	7.00424	0.009
Stasis-GRW	2.281291	5	8.437418	20.789781	0.000
$\delta^{18}O$	9.015465	3	-10.940022	1.412342	0.145
pcPa	9.114587	3	-11.138266	1.214098	0.161

4.5.4. Famennian record, Polygnathus. – Two models were very close in fitting *Polygnathus* size evolution at CT, corresponding either to an unbiased random walk or evolution towards an adaptive peak (Ohrstein-Uhlenbeck) (Table 10). In BU, the best model was by far the stasis (Table 11). In both cases, this suggested an overall stability of size throughout the record, with possibly a phase of initial evolution towards this adaptive peak that could be documented in CT due to the more extensive record in the early Famennian compared to BU where this period is missing (Fig. 7B).

Table 10. Comparison of support for each model of *Polygnathus* evolution in CT (comparing 11 models [n = 21, method = joint]. LogL= model log likelihood, K = number of model parameters, AICc = Akaike's Information Criterion corrected for small sample size, dAICc = difference in AICc score between the best model and the model being compared, Akaike.wt: Akaike weights (proportion of the total amount of predictive power).

	logL	K	AICc	dAICc	Akaike.wt
GRW	7.300514	3	-7.189263	3.406202	0.049
URW	7.244408	2	-9.822149	0.7733159	0.182
Punc-1	7.719622	4	-4.939243	5.6562214	0.016
OU	**10.547732**	**4**	**-10.595465**	**0.000000**	**0.268**

Stasis	6.643551	2	-8.620435	1.9750297	0.100
URW-Stasis	11.053871	5	-8.107743	2.4877218	0.077
Stasis-URW	9.91964	4	-9.33928	1.2561847	0.143
GRW-Stasis	11.100333	6	-4.200666	6.3947989	0.011
Stasis-GRW	9.954323	5	-5.908646	4.6868189	0.026
$\delta^{18}O$	6.645781	3	-5.879798	4.715667	0.025
pcPa	8.047335	3	-8.682905	1.9125599	0.103

Table 11. Comparison of support for each model of *Polygnathus* evolution in BU (comparing 6 models [n = 17, method = joint]. LogL= model log likelihood, K = number of model parameters, AICc = Akaike's Information Criterion corrected for small sample size, dAICc = difference in AICc score between the best model and the model being compared, Akaike.wt: Akaike weights (proportion of the total amount of predictive power).

	logL	K	AICc	dAICc	Akaike.wt
GRW	-4.89080337	3	17.627761	12.212885	0.001
URW	-4.92236396	2	14.701871	9.286995	0.005
OU	2.13569649	4	7.06194	1.647064	0.225
Stasis	**-0.27886661**	**2**	**5.414876**	**0.000000**	**0.512**
$\delta^{18}O$	-0.27475861	3	8.395671	2.980795	0.115
pcPa	-0.07352906	3	7.993212	2.578336	0.141

5. Discussion

5.1. "Temperature – Size Relationship" – A rule valid at a larger geographic scale ?

In this review of ten datasets documenting paleotemperature vs conodont size variation, the temperature-size rule (TSR) was supported in one case only, corresponding to the geographic variation during the *linguiformis* time slice. This case by far involved the largest range of paleotemperature variation ($\delta^{18}O$ range ~ 4‰), twice as large as the largest range of temporal variation among the records involved here ($\delta^{18}O$ range ~ 2‰ along the Famennian record at CT). Further in line with the TSR hypothesis, conodonts (both *Palmatolepis* and *Polygnathus*) tended to be larger during the Famennian in CT than in BU, characterized by warmer environment.

Possibly, consistent shifts in life history traits, leading to the TSR signature, may only arise as large-scale patterns. In agreement, during the *linguiformis* zone, different kinds of size-frequency distributions were found for *Palmatolepis* between the Western Paleotethys, characterized by highly skewed distributions, and the Eastern Paleotethys, with flatter distributions characterized by a more balanced contribution of small and large specimens, and the occurrence of largest specimens (Girard et al. 2007). These environments, located on the eastern shelves of Paleotethys (Northern Australia) were offshore of stromatoporoid reefs. In modern oceans, the presence of symbiont-bearing reefs

usually indicates conditions with low levels of nutrient content and primary productivity, associated with clear waters favoring the development of photosymbionts (Wood 1993; Humphreys et al. 2018). Such conditions might have reinforced the TSR, with warm oligotrophic waters offering less resources for growth, and hence leading to smaller conodonts (Girard at al. 2007).

5.2. Size distribution in conodonts – what biological processes beyond?

The concept of TSR has been developed for describing animal's growth at different temperatures (Atkinson 1994). By transferring the TSR to conodonts, one tacitly assumes that the size of the elements found in the fossil record approximate body size (Purnell 1993). This hypothesis may be valid given the continuous growth of the conodont elements, through addition of thin lamellae along the life of the former animal. It remains that the frequency of accretion of new lamellae is unknown, and might have varied with the age of the animal, and the environmental conditions.

According to the TSR, the animal's growth is accelerated in warm waters, leading to younger animals reaching maturity at a smaller size. In cold waters, animals would grow slower and but ultimately reach larger size. As a consequence, size-frequency distribution for cold water animals should be flatter and reach larger maximal size. Assuming that in conodonts, element size approximates body size, the size-frequency distribution in an assemblage records another parameter, namely the pattern of reproduction: abundant production of small-sized juveniles should heavily contribute to skewed distributions, with a peak of small-sized elements (Fig. 8). Such differences in life-history traits have been evoked to explain differences in the shape of the size-frequency distribution between *Palmatolepis* and *Ancyrodella* in the Late Frasnian (Girard & Renaud 2008) as it has been observed on two branchiopod (crustaceans) species (Huang & Chou 2017). Such dynamics might interfere with the TSR sensu stricto, and even if biologically valid, make it difficult to be detected in the fossil record.

5.3. Local conditions interfering with global trends

If a TSR-like pattern was found across the Paleotethys, the trend was not validated at a smaller geographic scale among the sections from the Western Paleotethys. The sections LSC and CUQ were relatively close to each other, and both characterized by colder waters than the Moroccan Mrirt section. Yet, LSC is characterized by the smallest-sized distribution. This section is characterized throughout by poorly oxygenated conditions (Girard & Renaud 2007). Oxygen supply is an important factor controlling body size of marine organisms. The challenge of oxygen supply being more acute at high temperature, and for large body size, this may explain why animals grow to smaller size in warm waters, oxygen supply has been invoked as the main driver of the TSR itself (Forster et al. 2012). Anoxic environments may represent cases where limitation in oxygen supply is not driven primarily

by water temperature, leading to deviation from the TSR. Further arguing in this direction, the level experiencing a punctuation towards smaller *Palmatolepis* size in LSC corresponds to the onset of anoxic facies in the section. However, the paucity of anoxic levels in most of the sections considered in the present study precluded to further disentangle the importance of decreased oxygen supply due to increasing water temperature or local anoxic conditions on conodont size. An alternate explanation would be the ability of organisms to adjust their physiology to such oxygen limitation at high temperature, at least within the range of tolerance of the concerned group (Einum et al. 2021).

5.4. Reverse TSR during stressful periods – nanism counterbalancing TSR?

A significant relationship between conodont size and paleotemperature proxy was found in few other cases: *Palmatolepis* during the Late Frasnian at CUQ and along the Famennian at CT; and possibly in *Ancyrodella* at CUQ. Results derived from linear models and the comparison of evolutionary modes were on this respect very congruent. The linear mixed effect model including all specimens in the analysis, but integrating the level as random factor appeared as especially efficient in retrieving the correlation in *Ancyrodella* at CUQ, that also emerge as highly probable using the comparison of evolutionary modes. Using the correction for temporal auto-correlation failed to identify some otherwise consistent size – paleotemperature relationships (*Palmatolepis* during the Kellwasser period at CUQ, *Palmatolepis* during the Famennian at CT). Possibly, by correcting for temporal autocorrelation, the effect of congruent trends is discarded, that however correspond to biologically relevant covariation between variables.

However, in all these cases where the size – paleotemperature relationship emerged as consistently supported, the direction of the relationship was reverse to the expectations of the TSR: size decreased with increasing $\delta^{18}O$ and hence with decreasing temperature.

The Late Frasnian was punctuated by two major anoxic events, the Lower and Upper Kellwasser events, the later culminating in the mass extinction punctuating the Frasnian / Famennian boundary. The events LKW and UKW were associated with cooling phases (Joachimski & Buggisch 2002), leading to a morphological response of *Palmatolepis* (Balter et al. 2008). The trends reported here suggest that *Palmatolepis* and possibly *Ancyrodella* responded to these short-term cooling phases by a decrease in size, and not an increase as expected by the TSR. The Kellwasser events, especially the UKW, were associated with extinctions pointing to momentary destabilization of the marine faunas (Racki 1998; Barash 2016). Disruption of food chains are prone to drive size reduction in various organisms (Rita et al. 2019; He et al. 2010). In this case, external driver related to available resources would override the effects related water temperature in determining size evolution.

5.5. A threshold response to temperature?

509 The reverse TSR during the Late Frasnian at CUQ was however not supported in the two other
510 sections documented, LSC and Mrirt, where little size variation was observed. A possible explanation
511 would be that conodont size responded to temperature decrease only below a certain threshold. The
512 range of paleotemperature variations was not more important at CUQ as at Mrirt and LSC, but it was
513 shifted towards colder temperatures. A threshold of temperature tolerance might thus have been
514 crossed in CUQ during cold phases but not in the warmer conditions of LSC and Mrirt, explaining why
515 conodont size responded to temperature variation in CUQ only. A similar process might be
516 responsible for the patterns observed during the Famennian, with a significant size-temperature
517 relationship observed at CT but not at BU. The threshold for the temperature response (~18‰ $\delta^{18}O$)
518 might have been passed in the colder CT but not in the warmer BU, where the range of
519 paleotemperature variation was anyway reduced (Girard et al. 2020).
520 The differential response of genera like *Palmatolepis* and *Polygnathus* might be due to different
521 temperature tolerance, although they are mostly known for preference regarding water depth /
522 distance to the shore (Seddon & Sweet 1971; Klapper & Barrick 1975; Sandberg 1976). During the
523 Famennian, *Polygnathus* might have displayed a wider tolerance to temperature than *Palmatolepis*,
524 explaining the different patterns for the two coexisting genera. This hypothesis is supported by the
525 fact that *Polygnathus* flourished in the icehouse Carboniferous context, while *Palmatolepis* went
526 extinct during the crisis punctuating the Devonian/Carboniferous boundary.
527
528 *5.6. An unknown forcing to Palmatolepis size evolution in the Famennian*
529 Two alternate strategies were explored to test for the TSR hypothesis: exploring the correlation
530 between size and paleotemperature records, or modelling modes of size evolution, among which
531 tracking an environmental variable. Both approaches agreed when a temperature-size relationship
532 was strongly supported (Late Frasnian *Palmatolepis* at CUQ). However, evolutionary models further
533 allowed to explicitly test for alternate scenarios, such as punctuation or stasis. Comparing such
534 models is only relevant for sequences with a sufficient number of levels, allowing to integrate modes
535 of evolution involving switch from one mode to another.
536 This was the case for the Famennian sequence (more than 10 My), and the separate analysis of the
537 CT and BU record of *Palmatolepis* size delivered amazingly congruent results, suggesting a sudden
538 decrease in size at ~369.7 Ma. The congruence in both outcrops suggests a common environmental
539 forcing.
540 It antedates a shift in detrital supply observed in several outcrops from the NW Paleotethys during
541 the early *marginifera* Zone, dated earlier as 368 Ma (Girard et al. 2021). This abrupt shift in detrital
542 supply is interpreted as due to a remnant oceanic barrier vanishing during the early middle
543 Famennian due to sea-level changes and/or tectonic events. Response of marine fauna to such

544 modifications in water masses exchanges can antedate the final closure or opening, as exemplified by
545 deep-water foraminifera being affected earlier by the closure of the Panama Isthmus compared to
546 shallow-water species (Schmidt et al 2016). Such a dynamic regarding *Palmatolepis* response remains
547 highly speculative given the poor knowledge of the timing of the different processes involved.
548 More simply, the shifts in the size record of *Palmatolepis* could match the onset of the temperature
549 decrease that will characterize the second part of the Famennian. It may have triggered an evolution
550 towards a new adaptive optimum after an initial phase of random walk following the
551 Frasnian/Famennian crisis; the paucity of the record during the early Famennian in BU probably
552 limited the assessment of the evolutionary mode during the initial phase.
553 The critical time of ~369.5 Ma also corresponds to a pivotal point after which the relative abundance
554 of *Palmatolepis* decreases (Girard et al. 2020). With a wider tolerance to temperature, *Polygnathus*
555 would have been little affected, explaining its stable size through the record. The case of these two
556 contrasted responses to the Famennian environmental changes highlight that the TSR hypothesis, for
557 being seducing, constitutes an oversimplification of complex eco-evolutionary processes.
558
559 **Declaration of competing interest**
560 The authors declare that they have no conflict of interest.
561
562 **Acknowledgements**
563 We warmly thank Sandrine Le Houedec for acquisition of the oxygen isotope data (Mrirt, Vietnam).
564 This research was supported by a French ANR grant (ANR-13-BSV7-005). This is publication ISEM 202x-
565 xxx.
566
567
568
569 **References**
570 Aldridge, R.J., Briggs, D.E.G., Smith, M.P., Clarkson, E.N.K., Clark, N.D.L., 1993. The anatomy of conodonts.
571 Philosophical Transactions of the Royal Society 340, 405-421.
572 Ashton, K., Tracy, M.C., Queiroz, A.D., 2000. Is Bergmann's rule valid for mammals? American Naturalist 156,
573 390–415.
574 Atkinson, D., 1994. Temperature and Organism Size—A Biological Law for Ectotherms? in: Begon, M., Fitter,
575 A.H. (Eds.), Advances in Ecological Research. Academic Press, pp. 1-58.
576 Atkinson, D., Morley, S.A., Hughes, R.N., 2006. From cells to colonies: at what levels of body organization
577 does the 'temperature-size rule' apply? Evolution & Development 8, 202-214.
578 https://doi.org/10.1111/j.1525-142X.2006.00090.x
579 Balter, V., Renaud, S., Girard, C., Joachimski, M.M., 2008. Record of climate-driven morphological changes in
580 376 Ma Devonian fossils. Geology 36, 907-910.
581 Balter, V., Martin, J., Tacail, T., Suan, G., Renaud, S., Girard, C., 2019. Ca stable isotopes place Devonian
582 conodonts as first level carnivores. Geochemical Perspectives Letters 10, 36-39.
583 Barash, M.S. 2016. Causes of the great mass extinction of marine organisms in the Late Devonian.
584 Oceanology 56, 863–875. https://doi.org/10.1134/S0001437016050015

585 Beaulieu, J.M., Jhuwueng, D.-C., Boettiger, C., O'Meara, B.C., 2012. Modeling stabilizing selection: expanding
586 the Ornstein–Uhlenbeck model of adaptive evolution. Evolution 66, 2369–2383.
587 Bergmann, C., 1847. Über die Verhältnisse der Warmekonomie der Tiere zu ihrer Grösse. Göttinger Studien 3,
588 595-708.
589 Bonhomme, V., Picq, S., Gaucherel, C., Claude, J., 2014. Momocs: Outline Analysis Using R. Journal of
590 Statistical Software 56, 1 - 24.
591 Briggs, D.E.G., Clarkson, E.N.K., Aldridge, R.J., 1983. The conodont animal. Lethaia 16, 1-14.
592 Buggisch, W., Joachimski, M.M., Sevastopulo, G., Morrow, J.R., 2008. Mississippian $\delta^{13}C_{carb}$ and conodont
593 apatite $\delta^{18}O$ records — Their relation to the Late Palaeozoic Glaciation. Palaeogeography Palaeoclimatology
594 Palaeoecology 268, 273-292.
595 Butler, M.A., King, A.A., 2004. Phylogenetic comparative analysis: a modelling approach for adaptive
596 radiation. American Naturalist 164, 683–695.
597 Donoghue, P.C.J., Purnell, M.A., 1999. Mammal-like occlusion in conodonts. Paleobiology 25, 58-74.
598 Einum, S., Bech, C., Kielland, Ø.N., 2021. Quantitative mismatch between empirical temperature-size rule
599 slopes and predictions based on oxygen limitation. Scientific Reports 11, 23594.
600 Forster, J., Hirst, A.G., Atkinson, D., 2012. Warming-induced reductions in body size are greater in aquatic
601 than terrestrial species. Proceedings of the National Academy of Sciences 109, 19310-19314.
602 Girard, C., Renaud, S., Sérayet, A., 2004. Morphological variation of *Palmatolepis* Devonian conodonts:
603 species *vs*. genus. Comptes rendus Palevol 3, 1-8.
604 Girard, C., Renaud, S., 2007. Quantitative conodont-based approaches for correlation of the Late Devonian
605 Kellwasser events. Palaeogeography Palaeoclimatology Palaeoecology 250, 114-125.
606 Girard, C., Renaud, S., Feist, R., 2007. Morphometrics of Late Devonian conodont genus *Palmatolepis*:
607 phylogenetic, geographical and ecological contributions of a generic approach. Journal of
608 Micropalaeontology 26, 61-72.
609 Girard, C., Renaud, S., 2008. Disentangling allometry and response to Kellwasser anoxic events in the Late
610 Devonian conodont genus *Ancyrodella*. Lethaia 41, 383-394.
611 Girard, C., Ta, H.P., Savage, N.M., Renaud, S., 2010. Temporal dynamics of the geographic differentiation of
612 Late Devonian *Palmatolepis* assemblages in the Prototethys. Acta Paleontologica Polonica 55, 675-687.
613 Girard, C., Renaud, S., 2012. Disparity changes in 370 Ma Devonian fossils: the signature of ecological
614 dynamics? PLoS ONE 7, e36230.
615 Girard, C., Cornée, J.-J., Corradini, C., Fravalo, A., Feist, R., 2014. Palaeoenvironmental changes at Col des
616 Tribes (Montagne Noire, France), a reference section for the Famennian of north Gondwana-related areas.
617 Geological Magazine 151, 864-884.
618 Girard, C., Cornée, J.-J., Charruault, A.-L., Corradini, C., Weyer, D., Bartzsch, K., Joachimski, M.M., Feist, R.,
619 2017. Conodont biostratigraphy and palaeoenvironmental trends during the Famennian (Late Devonian) in
620 the Thuringian Buschteich section (Germany). Newsletters on Stratigraphy 50, 71-89.
621 Girard, C., Cornée, J.-J., Joachimski, M.M., Charruault, A.-L., Dufour, A.-B., Renaud, S., 2020. Paleogeographic
622 differences in temperature, water depth and conodont biofacies during the Late Devonian.
623 Palaeogeography Palaeoclimatology Palaeoecology 549. https://doi.org/10.1016/j.palaeo.2018.06.046
624 Girard, C., Feist, R., Mossoni, A., Cornée, J.-J., Camps, P., Charruault, A.-L., Corradini, C., 2021. North-
625 Gondwana – Laurussia dynamic paleogeography challenged by magnetic susceptibility through the
626 Famennian. Gondwana Research 97, 263-272.
627 Hansen, T.F., 1997. Stabilizing selection and the comparative analysis of adaptation. Evolution 51, 1341–
628 1351.
629 He, W.-H., Twitchett, R.J., Zhang, Y., Shi, G.R., Feng, Q.-L., Yu, J.-X., Wu, S.-B., Peng, X.-F., 2010. Controls on
630 body size during the Late Permian mass extinction event. Geobiology 8, 391-402.
631 Horne, C.R., Hirst, A.G., Atkinson, D., 2015. Temperature-size responses match latitudinal-size clines in
632 arthropods, revealing critical differences between aquatic and terrestrial species. Ecology Letters 18, 327-
633 335.
634 Horne, C.R., Hirst, A.G., Atkinson, D., 2017. Seasonal body size reductions with warming covary with major
635 body size gradients in arthropod species. Proceedings of the Royal Society B: Biological Sciences 284,
636 20170238.

637 Huang, W.-P., Chou, L.-S., 2017. Temperature effects on life history traits of two sympatric branchiopods
638 from an ephemeral wetland. PLoS ONE 12, e0179449.
639 Humphreys, A.F., Halfar, J., Ingle, J.C., Manzello, D., Reymond, C.E., Westphal, H., Riegl, B., 2018. Effect of
640 seawater temperature, pH, and nutrients on the distribution and character of low abundance shallow water
641 benthic foraminifera in the Galápagos. PLoS ONE 13, e0202746.
642 Hunt, G., 2006. Fitting and comparing models of phyletic evolution: random walks and beyond. Paleobiology
643 32, 578-501.
644 Hunt, G., Bell, M., Travis, M. 2008. Evolution toward a new adaptive optimum: Phenotypic evolution in a
645 fossil stickleback lineage. Evolution 62(3), 700-710.
646 Hunt, G., Carrano, M.T., 2010. Models and methods for analyzing phenotypic evolution in lineages and
647 clades. The Paleontological Society Papers 16, 245–269.
648 Hunt, G., 2014. Modeling evolution in paleontological time-series. Version 0.4-5. Available at cran.r-
649 project.org/web/packages/paleoTS/.
650 Janvier, P., 1995. Conodonts join the club. Nature 374, 761-762.
651 Joachimski, M., Buggisch, W., 2002. Conodont apatite $\delta^{18}O$ signatures indicate climatic cooling as a trigger of
652 the Late Devonian mass extinction. Geology 30, 711-714.
653 Joachimski, M.M., Breisig, S., Buggisch, W., Talent, J.A., Mawson, R., Gereke, M., Morrow, J.R., Day, J.,
654 Weddige, K., 2009. Devonian climate and reef evolution: Insights from oxygen isotopes in apatite. Earth and
655 Planetary Science Letters 284, 599-609.
656 Klapper, G., Barrick, J.E., 1978. Conodont ecology: pelagic versus benthic. Lethaia 11, 15-23.
657 Koike, T., 1992. Morphological variation in Spathian conodonts *Spathoicriodus collinsoni* (Solien) from the
658 Taho Limestone, Japan, in: Ishizaki, K., Saito, T. (Eds.), Centenary of Japanese Micropaleontology. Terra
659 Publishing Compagny, Tokyo, pp. 355-364.
660 Le Houedec, S., Girard, C., Balter, V., 2013. Conodont Sr/Ca and $\delta^{18}O$ record seawater changes at the
661 Frasnian–Famennian boundary. Palaeogeography Palaeoclimatology Palaeoecology 376, 114-121.
662 https://doi.org/10.1016/j.palaeo.2013.02.025
663 McGhee, G.R.J., 1996. The Late Devonian Mass Extinction - The Frasnian/Famennian crisis. Columbia
664 University Press, New York.
665 Olson, V.A., Davies, R.G., Orme, C.D., Thomas, G.H., Meiri, S., Blackburn, T.M., Gaston, K.J., Owens, I.P.,
666 Bennett, P.M., 2009. Global biogeography and ecology of body size in birds. Ecology Letters 12, 249-259.
667 Pinheiro J, Bates D, DebRoy S, Sarkar D, R Core Team. 2018 nlme: linear and nonlinear mixed effects models.
668 R package version 3.1-137. See https://CRAN.R-project.org/package=nlme.
669 Purnell, M.A., 1993. Feeding mecanisms in conodonts and the function of the earliest vertebrate hard tissues.
670 Geology 21, 375-377.
671 Purnell, M.A., 1994. Skeletal ontogeny and feeding mechanisms in conodonts. Lethaia 27, 129-138.
672 R-Core-Team, 2018. A language and environment for statistical computing. Vienna: R Foundation for
673 Statistical Computing. http://www.R-project.org.
674 Racki, G., 1998.Frasnian–Famennian biotic crisis: undervalued tectonic control? Palaeogeography,
675 Palaeoclimatology, Palaeoecology 141(3–4), 177-198, https://doi.org/10.1016/S0031-0182(98)00059-5.
676 Renaud, S., Girard, C., 1999. Strategies of survival to extreme environmental perturbations: evolution of
677 conodonts in response to the Kellwasser crisis (Upper Devonian). Palaeogeography Palaeoclimatology
678 Palaeoecology 146, 19-32.
679 Renaud, S., Ecalle, B., Claisse, P., Charruault, A.-L., Ledevin, R., Girard, C., 2021. Patterns of bilateral
680 asymmetry and allometry in Late Devonian *Polygnathus* conodonts. Palaeontology 67(1), 137-159.
681 https://doi.org/10.1111/pala.12513
682 Renaud, S., Michaux, J., Mein, P., Aguilar, J.-P., Auffray, J.-C., 1999. Patterns of size and shape differentiation
683 during the evolutionary radiation of the European Miocene murine rodents. Lethaia, 32, 61-71.
684 Rita, P., Nätscher, P., Duarte, L.V., Weis, R., De Baets, K., 2019. Mechanisms and drivers of belemnite body-
685 size dynamics across the Pliensbachian–Toarcian crisis. Royal Society open Science 6, 190494.
686 Rodriguez, M.A., Olalla-Tarraga, M.A., Hawkins, B.A., 2008. Bergmann's rule and the geography of mammal
687 body size in the Western Hemisphere. Global Ecology and Biogeography 17, 274-283.
688 Rollinson, N., Rowe, L., 2018. Temperature-dependent oxygen limitation and the rise of Bergmann's rule in

689 species with aquatic respiration. Evolution 72, 977-988.
690 Salamon, M.A., Brachaniec, T., Kołbuk, D., Saha, A., Gorzelak, P., 2021. Shared patterns in body size declines
691 among crinoids during the Palaeozoic extinction events. Scientific Reports 11, 20351.
692 Sandberg, C.A., 1976. Conodont biofacies of late Devonian *Polygnathus styriacus* Zone in western United
693 States, in: Barnes, C.R. (Ed.), Conodont Paleoecology. Geological Association of Canada special Paper,
694 Montreal, pp. 171-186.
695 Schmidt, D.N., Lazarus, D., Young, J.R., Kucera, M., 2006. Biogeography and evolution of body size in marine
696 plankton. Earth-Science Reviews 78, 239-266.
697 Schmidt, D., Caromel, A., Seki, O., Rae, J.W.B., Renaud, S., 2016. Morphological response of planktic
698 foraminifers to habitat modifications associated with the emergence of the Isthmus of Panama. Marine
699 Micropaleontology 128, 28-38.
700 Scott, A.C., Collinson, C., 1959. Intraspecific variability in conodonts: *Palmatolepis glabra* Ulrich & Bassler.
701 Journal of Paleontology 33, 550-565.
702 Seddon, G., Sweet, W.C., 1971. An ecologic model for conodonts. Journal of Paleontology 45, 869-880.
703 Sheets, H.D., Mitchell, C., 2010. Why the null matters: statistical tests, random walks and evolution. Genetica,
704 112– 113:105–125.
705 Sheridan, J.A., Bickford, D., 2011. Shrinking body size as an ecological response to climate change. Nature
706 Climate Change 1, 401-406.
707 Shirley, B., Grohganz, M., Bestmann, M., Jarochowska, E., 2018. Wear, tear and systematic repair: testing
708 models of growth dynamics in conodonts with high-resolution imaging. Proceedings of the Royal Society B:
709 Biological Sciences 285.
710 Slice, D., Bookstein, F.L., Marcus, L., Rohlf, F.J., 1996. Appendix I. A glossary for geometric morphometrics.
711 NATO ASI Serie A: Life Sciences 284, 531-552.
712 Spalletta, C., Perri, M.C., Over, D.J., Corradini, C., 2017. Famennian (Upper Devonian) conodont zonation:
713 revised global standard. Bulletin of Geosciences 92, 1-27.
714 Sun, Y., Li, M., Song, G., Lei, F., Li, D., Wu, Y., 2017. The role of climate factors in geographic variation in body
715 mass and wing length in a passerine bird. Avian Research 8, 1.
716 Twitchett, R.J., 2006. The palaeoclimatology, palaeoecology and palaeoenvironmental analysis of mass
717 extinction events. Palaeogeography Palaeoclimatology Palaeoecology 232, 190-213.
718 Walczyńska, A., Sobczyk, Ł., 2017. The underestimated role of temperature–oxygen relationship in large-scale
719 studies on size-to-temperature response. Ecology and Evolution 7, 7434-7441.
720 Walliser, O.H., 1996. Global events and event stratigraphy. Springer Verlag, Berlin, Heidelberg, New York.
721 Wood, R., 1993. Nutrients, Predation and the History of Reef-Building. Palaios 8, 526-543.
722 Zhang, X., Joachimski, M.M., Yiming, G., 2021. Late Devonian greenhouse-icehouse climate transition: New
723 evidence from conodont δ18O thermometry in the eastern Palaeotethys (Lali section, South China).
724 Chemical Geology 581. https://doi.org/10.1016/j.chemgeo.2021.120383.
725 Zhang, X., Li, S., Song, Y., Gong, Y., 2020. Size reduction of conodonts indicates high ecological stress during
726 the late Frasnian under greenhouse climate conditions in South China. Palaeogeography Palaeoclimatology
727 Palaeoecology 556. https://doi.org/10.1016/j.palaeo.2020.109909.
728 Ziegler, W., Sandberg, C.A., 1990. The late Devonian standard conodont zonation. Courier Forschung-Institut
729 Senckenberg 121, 1-115.
730

Supplementary Tables: data per section and per genus. P Wilcox: probabilities of pairwise size differences between successive levels along a section (pairwise Wilcoxon tests). In bold, P < 0.01, in italics P < 0.05.

Whole Kellwasser Period - CUQ

Palmatolepis	Age	$\delta^{18}O$	N	LogA0	SD	P Wilcox
CUQ23d	373.6	17.6	121	0.044	0.355	
CUQ23e	373.5	17.4	18	0.377	0.388	**0.0008**
CUQ24a	373.4	17.5	37	0.153	0.383	*0.0410*
CUQ24bc	373.2	18.2	15	0.362	0.472	0.1984
CUQ24d	373.1	18.3	19	0.036	0.257	0.0709
CUQ24e	372.9	18.4	34	0.203	0.279	*0.0232*
CUQ25b	372.8	17.5	48	0.062	0.301	*0.0461*
CUQ25cd	372.7	18.1	49	0.039	0.312	0.3942
CUQ26b	372.5	18.2	235	0.199	0.413	*0.0110*
CUQ27	372.4	17.9	170	0.173	0.319	0.8133
CUQ28c	372.2	17.9	263	0.256	0.362	*0.0231*
CUQ29b	372.1	17.6	350	0.307	0.416	0.2739
CUQ30a	372.0	17.5	469	0.290	0.376	0.8425
CUQ31c	371.8	17.2	481	0.204	0.359	**0.0005**
CUQ31f	371.7	17.1	94	0.428	0.337	**0.0000**
CUQ31g1	371.5	16.7	68	0.473	0.363	0.5180
CUQ31g2	371.4	16.9	58	0.492	0.420	0.5423
CUQ32a	371.1	17.4	51	0.280	0.296	**0.0019**
CUQ32b	370.9	17.3	45	0.240	0.229	0.5471

Whole Kellwasser Period - Mrirt

Palmatolepis	Age	$\delta^{18}O$	N	LogA0	SD	P Wilcox
M01	373.8	16.5	63	0.323	0.354	
M02	373.6	16.3	200	0.190	0.421	**0.0043**
M03	373.4	16.9	71	0.264	0.370	0.1423
M05	373.0	16.6	59	0.413	0.424	*0.0283*
M06	372.8	16.5	420	0.224	0.332	**0.0010**
M07	372.5	16.2	81	0.151	0.395	*0.0197*
M08	372.3	16.0	74	0.091	0.383	0.2931
M09	372.0	15.6	52	0.186	0.336	0.0717
M11a	371.8	16.0	13	0.246	0.546	0.9673
M11b	371.5	15.9	25	0.302	0.381	0.4653
M12	371.0	16.1	6	0.150	0.314	0.5095
M13	370.8	16.3	133	0.164	0.333	0.9876
M15a	370.4	15.9	98	0.273	0.389	*0.0499*

Whole Kellwasser Period - LSC

Palmatolepis	Age	$\delta^{18}O$	N	LogA0	SD	P Wilcox
LSC03A	373.9	16.9	28	0.081	0.397	
LSC04D	373.8	17.0	13	0.058	0.339	0.8574
LSC05A	373.7	16.7	11	-0.138	0.316	0.1863
LSC06A	373.6	16.8	115	0.168	0.399	*0.0171*

LSC07C	373.5	16.4	18	0.063	0.432	0.2102
LSC08C	373.4	17.0	8	0.178	0.175	0.1147
LSC09B	373.2	17.4	11	-0.100	0.167	**0.0068**
LSC10A	373.0	17.9	47	-0.033	0.327	0.9377
LSC11B	372.7	17.2	89	0.106	0.401	*0.0104*
LSC12	372.5	17.2	251	0.029	0.394	0.0510
LSC13A	372.4	16.8	799	0.083	0.383	*0.0211*
LSC13B	372.2	16.4	934	0.067	0.361	0.7505
LSC13C	372.0	16.4	264	0.001	0.331	*0.0189*
LSC14B	371.8	16.1	95	-0.017	0.398	0.2478
LSC14C2	371.6	16.3	27	0.182	0.388	*0.0127*
LSC14D	371.4	16.5	13	0.066	0.300	0.3602
LSC14F1	371.1	17.2	94	0.445	0.304	**0.0002**
LSC14F2	370.9	17.1	48	0.209	0.365	**0.0000**
LSC14G	370.8	16.9	8	0.413	0.204	*0.0302*
LSC14H	370.6	16.9	226	0.221	0.383	0.0755
LSC15A	370.5	16.7	79	0.123	0.382	*0.0458*

Whole Kellwasser Period - CUQ

Ancyrodella	Age	$\delta^{18}O$	N	LogA0	SD	P Wilcox
CUQ23D	373.6	17.6	4	0.466	0.390	
CUQ23D2	373.6	17.6	7	0.224	0.360	0.3152
CUQ23e	373.5	17.4	11	0.237	0.392	1.0000
CUQ24a	373.4	17.5	39	0.292	0.342	0.5024
CUQ24BC	373.2	18.2	4	0.013	0.096	0.1305
CUQ24E	372.9	18.4	3	0.408	0.154	0.0571
CUQ25b	372.8	17.5	7	0.327	0.276	0.5167
CUQ25C	372.7	18.1	3	0.772	0.252	0.1167
CUQ26b	372.5	18.2	14	0.199	0.368	*0.0324*
CUQ27	372.4	17.9	5	0.680	0.151	*0.0143*
CUQ28c	372.2	17.9	16	0.375	0.369	*0.0401*
CUQ29b	372.1	17.6	16	0.457	0.383	0.5147
CUQ30	372.0	17.5	3	0.280	0.234	0.7121
CUQ31C	371.8	17.2	8	0.301	0.440	0.6303
CUQ31f	371.7	17.1	118	0.453	0.453	0.3496
CUQ31g1	371.5	16.7	10	0.880	0.369	**0.0062**
CUQ31g2	371.4	16.9	15	0.550	0.429	0.0709

Whole Kellwasser Period - Mrirt

Ancyrodella	Age	$\delta^{18}O$	N	LogA0	SD	P Wilcox
M01an	373.8	16.5	7	0.408	0.298	
M02an	373.6	16.3	18	0.493	0.310	0.5339
M03an	373.4	16.9	27	0.316	0.462	0.1425
M05an	373.0	16.6	6	0.237	0.341	0.7329
M06an	372.8	16.5	15	0.218	0.441	0.8500
M07an	372.5	16.2	20	0.616	0.494	*0.0116*
M09an	372.0	15.6	25	0.415	0.297	0.1616
M11an	371.8	16.0	6	0.336	0.496	0.7515

745

746 Famennian - *Palmatolepis* CT

747

	Age	$\delta^{18}O$	pcPa	N	LogA0	SD_LogA0	pWilcox
CT07	373.1	17.7	32.8	83	0.184	0.356	
CT11c	372.6	17.7	45.8	56	0.288	0.437	0.2186
CT22	371.8	17.4	62.9	95	0.506	0.321	**0.0001**
CT23	371.8	17.7	76.5	51	0.437	0.384	0.3493
CT24	371.1	17.7	67.4	53	0.471	0.315	0.7061
CT30	370.3	17.1	79.5	195	0.611	0.360	*0.0123*
CT32	369.9	17.6	94.4	52	0.626	0.318	0.9156
CT34	369.7	17.4	96.8	48	0.499	0.441	0.0650
CT35	369.6	18.0	97.3	235	0.289	0.405	**0.0025**
CT36	369.1	18.2	70.5	50	0.263	0.401	0.7132
CT37	368.7	17.5	98.4	88	0.265	0.404	0.9558
CT39	367.7	17.6	67.6	174	0.157	0.406	*0.0302*
CT41	367.6	17.7	89.2	89	0.163	0.292	0.3698
CT42	367.3	18.2	77.6	148	0.136	0.298	0.2218
CT48	366.2	18.2	97.5	42	0.045	0.282	**0.0090**
CT51	365.6	17.9	80.2	217	0.177	0.345	**0.0076**
CT52	365.3	17.8	62.3	23	0.190	0.373	0.8820
CT56	364.5	18.2	81.4	119	0.094	0.386	0.2190
CT59	364.3	19.1	75.0	92	0.194	0.313	*0.0111*
CT59-1	364.2	19.0	85.1	45	0.146	0.263	0.4292
CT61-1	363.0	19.2	51.9	64	0.116	0.259	0.3805
CT62	362.5	19.1	22.5	60	0.185	0.291	0.1069
CT63	362.3	19.2	29.1	106	0.362	0.354	**0.0039**
CT66	361.2	18.3	23.4	24	0.136	0.340	**0.0051**
CT69-1	360.6	19.0	8.8	11	0.389	0.351	*0.0345*
CT70-2	359.4	18.5	14.2	9	0.436	0.323	0.6027

748

749 Famennian - *Palmatolepis* BU

750

	Age	$\delta^{18}O$	pcPa	N	LogA0	SD_LogA0	Pwilcox
BU007	374.0	16.6	61.8	16	0.441	0.398	
BU010	373.1	16.5	67.9	7	0.066	0.474	*0.0469*
BU010G1	370.1	16.4	82.5	16	0.287	0.345	0.4515
BU011	370.1	16.9	76.9	209	0.413	0.450	0.2937
BU012	370.0	16.7	70.2	236	0.269	0.424	**0.0006**
BU018	369.6	17.2	96.7	50	0.273	0.372	0.5884
BU021	369.3	17.0	79.5	255	0.039	0.480	**0.0005**
BU025	368.7	17.0	97.8	442	-0.010	0.425	0.3421
BU029	368.3	17.0	94.1	391	-0.090	0.435	**0.0032**
BU035	367.7	17.3	86.9	60	0.406	0.404	**0.0000**
BU038	367.4	17.4	98.0	615	-0.106	0.377	**0.0000**
BU040	366.9	17.2	92.1	202	0.042	0.406	**0.0000**
BU044	366.7	17.1	92.2	340	-0.103	0.427	**0.0002**
BU051	366.2	17.6	96.5	254	-0.056	0.320	0.0770

BU055	365.9	17.8	95.3	177	-0.141	0.302	**0.0009**
BU060	365.5	16.7	89.9	71	0.094	0.317	**0.0000**
BU065	365.2	17.0	86.3	243	0.209	0.318	*0.0049*
BU069	364.9	17.8	81.2	125	-0.011	0.289	**0.0000**
BU076	364.3	17.8	62.6	137	0.059	0.382	0.1829
BU078	364.2	17.4	83.1	57	0.378	0.391	**0.0000**
BU082	363.8	17.9	51.8	70	0.139	0.404	*0.0013*
BU087	363.0	17.5	60.5	73	0.088	0.449	0.5221
BU093	362.4	17.7	58.5	53	0.363	0.413	**0.0020**
BU094	362.3	17.2	48.3	62	-0.042	0.385	**0.0000**
BU095	361.5	17.3	75.9	191	0.009	0.341	0.4926
BU103	360.2	17.3	37.4	18	0.182	0.411	0.1087

Famennian – *Polygnathus* CT

	Age	$\delta^{18}O$	pcPa	N	LogCS	SD_LogCS	Pwilcox
CT_007	373.1	17.7	32.8	180	6.259	0.375	
CT_011c	372.6	17.7	45.8	57	6.382	0.389	**0.0037**
CT_022	371.8	17.4	62.9	64	6.225	0.337	**0.0091**
CT_023	371.8	17.7	76.5	7	6.237	0.335	0.6365
CT_024	371.1	17.7	67.4	11	6.503	0.357	0.1042
CT_030	370.3	17.1	79.5	44	6.268	0.316	*0.0434*
CT_035	369.6	18.0	97.3	3	6.408	0.574	0.6352
CT_036	369.1	18.2	70.5	8	6.260	0.249	0.9212
CT_037	368.7	17.5	98.4	4	6.391	0.283	0.2828
CT_039	367.7	17.6	67.6	65	6.705	0.449	0.1695
CT_041	367.6	17.7	89.2	23	6.561	0.448	0.1745
CT_042	367.3	18.2	77.6	28	6.511	0.358	0.6728
CT_049	366.0	18.2	92.9	27	6.377	0.394	0.2510
CT_051	365.6	17.9	80.2	24	6.436	0.426	0.8151
CT_053	365.1	17.8	82.5	17	6.488	0.485	0.7436
CT_056	364.5	18.2	81.4	9	6.444	0.371	0.9579
CT_059	364.3	19.1	75.0	11	6.626	0.372	0.2947
CT_062	362.5	19.1	22.5	6	6.245	0.188	*0.0365*
CT_063	362.3	19.2	29.1	79	6.266	0.265	0.8570
CT_069-1	360.6	19.0	8.8	53	6.577	0.311	**0.0000**
CT_070-2	359.4	18.5	14.2	25	5.989	0.140	**0.0000**

Famennian - *Polygnathus* BU

	Age	$\delta^{18}O$	pcPa	N	LogCS	LogCS	P Wilcox
BU_012	370.0	16.7	70.2	12	6.697	0.386	
BU_021	369.3	17.0	79.5	53	6.275	0.367	**0.0019**
BU_025	368.7	17.0	97.8	2	6.379	0.402	0.6693
BU_029	368.3	17.0	94.1	9	5.863	0.222	0.1455
BU_035	367.7	17.3	86.9	5	6.634	0.441	**0.0010**
BU_038	367.4	17.4	98.0	14	6.315	0.511	0.2566
BU_040	366.9	17.2	92.1	98	6.176	0.352	0.3054
BU_044	366.7	17.1	92.2	26	6.540	0.473	**0.0005**
BU_051	366.2	17.6	96.5	10	6.181	0.465	*0.0255*

BU_055	365.9	17.8	95.3	7	6.656	0.381	*0.0330*
BU_060	365.5	16.7	89.9	16	6.214	0.270	**0.0046**
BU_065	365.2	17.0	86.3	45	6.135	0.322	0.4595
BU_069	364.9	17.8	81.2	20	6.088	0.554	0.2858
BU_076	364.3	17.8	62.6	15	6.271	0.455	0.1585
BU_082	363.8	17.9	51.8	3	6.166	0.138	0.6544
BU_093	362.4	17.7	58.5	2	6.948	0.398	0.2000
BU_103	360.2	17.3	37.4	10	6.347	0.265	0.1212

755